

Contact strength of monolithic and composite ceramic materials

L. Hegedüsová¹, L. Ceniga^{1*}, J. Dusza¹, M. Hnatko², P. Šajgalík²

¹*Institute of Materials Research, Slovak Academy of Sciences, Watsonova 47, 040 01 Košice, Slovak Republic*

²*Institute of Inorganic Chemistry, Slovak Academy of Sciences, Dúbravská cesta 9, 845 36 Bratislava, Slovak Republic*

Received 19 June 2009, received in revised form 9 September 2009, accepted 11 September 2009

Abstract

The paper deals with the determination of strength of ceramic materials and a microstructural analysis of strength-degrading defects. Strength is determined by mechanical tests in bending and contact modes. The bending and contact modes are simulated by a four-point bending test and single-cycle contact tests using rollers or spheres, respectively. The determination of strength is based on the Weibull analysis which is used for the determination of the characteristic strength σ_0 and the Weibull modulus m . Accordingly, numerical values of $\sigma_{0,\text{bend}}$ and $\sigma_{0,\text{cont}}$ related to the four-point bending test and the single-cycle contact test using rollers, respectively, enable to define a relationship between $\sigma_{0,\text{bend}}$ and $\sigma_{0,\text{cont}}$. Similarly, the same relationship is determined between numerical values of m_{bend} and m_{cont} . These relationships confirm the validity of the Fett's theory. In case of the bending mode, the strength-degrading defects are represented by flaws, which originate during the processing of a material. In case of the contact modes, different types of cracks, which are formed during mechanical loading, represent the strength-degrading defects. A detailed analysis of parameters of the cracks is also presented. The mechanical tests were applied to monolithic and composite ceramic materials represented by Si_3N_4 , SiC and $\text{MoSi}_2 + 10\% \text{Si}$, respectively.

Key words: nitrides, carbides, ceramic matrix composites, fracture, bending test, contact test

1. Introduction

Conventional tests used for the determination of strength of ceramic materials (e.g. three- or four-point bending tests) describe failure behaviour related to simple stress states. The simple stress states comprise mostly uniaxial stresses with relatively insignificant stress gradients. In case of practical applications, mechanical loading often leads to significantly inhomogeneous multi-axial stress states. In case of laboratory measurements, contact line or point loading can simulate the inhomogeneous multi-axial stress states. Two opposite rollers or two opposite spheres can induce the contact line or point loading, respectively.

In general, strength of ceramic materials is influenced by the presence of flaws, which originate during the material processing [1–6]. The determination of strength of ceramic materials is based on statistical methods, usually represented by the Weibull analysis

(see Section 2). The Weibull analysis results in the determination of the characteristic strength $\sigma_{0,\text{bend}}$ and $\sigma_{0,\text{cont}}$ along with the Weibull moduli m_{bend} and m_{cont} , related to the bending and contact modes, respectively. The determination of $\sigma_{0,\text{cont}}$, m_{cont} considers a theory valid for a single-cycle contact test using rollers or spheres proposed by Fett (see Eqs. (7), (9), (10)). Furthermore, the Fett's theory defines relationships between the Weibull parameters $\sigma_{0,\text{cont}}$, m_{cont} of the single-cycle contact test using rollers and the Weibull parameters $\sigma_{0,\text{bend}}$, m_{bend} of the four-point bending test (see Eqs. (6), (8)). Additionally, the relationships are verified by experimental results in Table 2 (see Section 5.2.1). Finally, in contrast to the experimental results in Table 2, no relationships between the Weibull parameters $\sigma_{0,\text{cont}}$, m_{cont} of the single-cycle contact test using spheres (see Section 5.2.2) and $\sigma_{0,\text{bend}}$, m_{bend} can be defined (see Table 3).

Strength of ceramic materials determined by the four-point bending test (see Sections 5.2.1, 5.2.2) and

*Corresponding author: tel: +421 557922 416; fax: +421 557922 408; e-mail address: lceniga@yahoo.com

the single-cycle contact test using rollers (see Section 5.2.2) is assumed to be influenced by the presence of flaws in a form of pores to represent fracture origins. The flaws arise during the processing and/or the specimen preparation (e.g. grinding). Additionally, the contact mode performed by rollers induces different types of cracks, i.e. lateral, median and contact end cracks (see Fig. 7).

The contact mode performed by spheres induces cone cracks to cause material failure (see Section 5.2.2), except of the ceramic material to exhibit a quasi-plastic character in compression. The quasi-plastic character in compression is assumed to be a reason of the initiation and the propagation of median cracks (see Fig. 12e). Stable growth of the cone cracks leads to higher values of m_{cont} compared with lower ones of m_{bend} . Accordingly, the higher values of m_{cont} correspond to significant preciseness of the determination of strength of ceramic materials. Additionally, the single-cycle contact test using spheres results in higher values of $\sigma_{0,\text{cont}}$ compared with those determined by the four-point bending test and the single-cycle contact test using rollers (see Tables 2, 3).

Finally, the contact test performed by spheres thus enables to obtain reproducible results. On the one hand, the determination requires large amount of specimens. On the other hand, the specimens are of small dimensions what is an advantage of this experimental technique, which is thus suitable for new developed ceramic materials.

2. Weibull analysis

Strength of a ceramic material is significantly influenced by the presence of flaws to originate during the processing. Accordingly, strength of a ceramic material is required to be determined by a suitable statistical function to consider the distribution of the flaws. The most used function to describe the distribution of flaws in a ceramic (brittle) material proposed by Weibull is derived as [7]

$$P_f = 1 - \exp \left[- \left(\frac{\sigma_i}{\sigma_0} \right)^m \right], \quad (1)$$

$$P_f = \frac{2i - 1}{2N}, \quad (2)$$

where P_f is probability of failure, N is number of measured values of the strength σ_i related to the i -th measurement, σ_0 is characteristic strength, m is a Weibull modulus. Additionally, the increase of the natural number i is required to correspond to the increase of a value of σ_i , i.e. $\sigma_i \leq \sigma_{i+1}$ for $i = 1, \dots, N$.

Equation (1) is transformed to the form

$$y = mx + a, \quad (3)$$

where y , x , a are derived as

$$y = \ln \left\{ \ln \left[\frac{2N}{2(N-i) + 1} \right] \right\},$$

$$x = \ln \sigma_i, \quad a = -m \ln \sigma_0. \quad (4)$$

A line with the tangent m can fit experimental values of y and x illustrated in the y - x -plot. With regard to Eq. (3) and the parameter a (see Eq. (6)), a point on the line with the coordinate $y = 0$ determines the coordinate $\ln \sigma = \ln \sigma_i$. The condition $y = 0$ results in the failure probability $P_f = (e - 1) / e = 0.632$, i.e. 63.2 %, and $e = 2.718282$ is the Euler number.

3. Fixtures for mechanical tests

3.1. Four-point bending test

A fixture used for the four-point bending test applied by the load P to the prismatic specimen 2 with the dimensions $W \times t \times L$ is shown in Fig. 1, where S_1 and S_2 are outer and inner spans, respectively. The strength σ_{bend} used for the determination of the characteristic strength $\sigma_{0,\text{bend}}$ by the Weibull analysis (see Section 2) has the form [7]

$$\sigma_{0,\text{bend}} = \frac{3P(S_1 - S_2)}{2tW^2}. \quad (5)$$

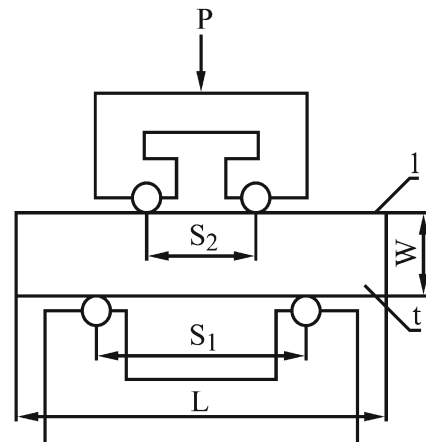


Fig. 1. A fixture used for the four-point bending test applied by the load P to the prismatic specimen 2 with the dimensions $W \times t \times L$.

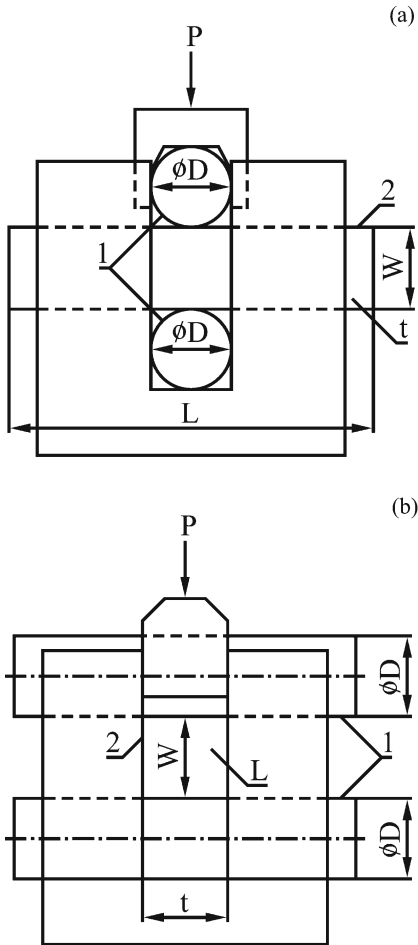


Fig. 2. Front (a) and side (b) views of a fixture used for the contact test using rollers 1 with the diameter D applied by the load P to the prismatic specimen 2 with the dimensions $W \times t \times L$.

3.2. Contact test using rollers

A fixture, designed by Fett [8–10], and used for the contact test using rollers, is shown in Fig. 2. The load P via the two opposite rollers 1 with the diameter D presses the prismatic specimen 2. As presented in [9, 10], a relationship between the characteristic strength $\sigma_{0,\text{bend}}$ and $\sigma_{0,\text{cont}}$ determined by the four-point bending test and the contact test using rollers, respectively, is derived as

$$\sigma_{0,\text{bend}} \approx \sigma_{0,\text{cont}}. \quad (6)$$

The characteristic strength $\sigma_{0,\text{cont}}$ is derived by the Weibull analysis (see Section 2) to consider the strength $\sigma_{0,\text{cont}}$. The strength $\sigma_{0,\text{cont}}$ is related to the value of the load P to cause failure of a material, and has the form [8–10]

$$\sigma_{0,\text{cont}} = \frac{0.98 P}{t W}. \quad (7)$$

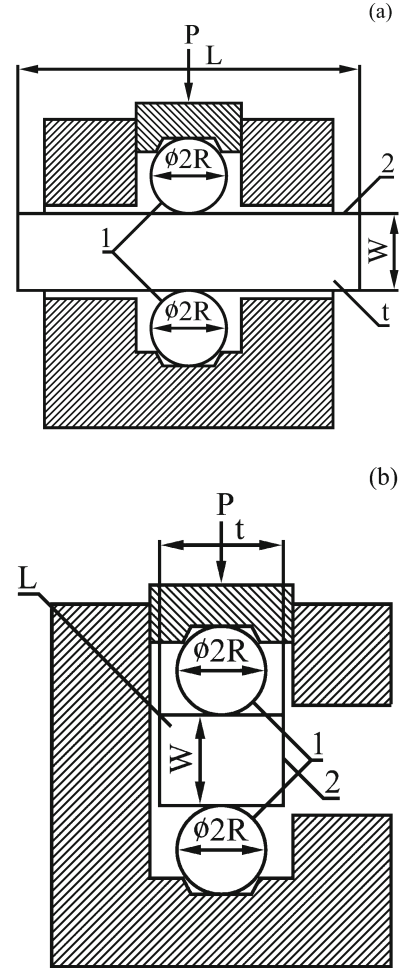


Fig. 3. Front (a) and side (b) cross-sections of a fixture used for the contact test using spheres 1 with the radius R applied by the load P to the prismatic specimen 2 with the dimensions $W \times t \times L$.

Similarly, the characteristic strength $\sigma_{0,\text{bend}}$ is derived by the Weibull analysis (see Section 2) to consider the strength σ_{bend} given by Eq. (5). Finally, a relationship between the Weibull moduli m_{bend} and m_{cont} is derived as [9, 10]

$$m_{\text{bend}} \approx 2m_{\text{cont}}, \quad (8)$$

where Eqs. (6), (8) represent the Fett's theory.

3.3. Contact test using spheres

A fixture, designed by Fett [8–10], and used for the contact test using spheres, is shown in Fig. 3. The load P via the two opposite spheres 1 with the radius R presses the prismatic specimen 2. The load P is transferred to the upper sphere by the roller 3 guided by the hollow roller 4. The contact test using spheres can be carried out using bending bars or fragments of shorter length.

The characteristic strength $\sigma_{0,\text{cont}}$ determined by the contact test using spheres is derived by the Weibull analysis (see Section 2) to consider the stress σ_{cont} in the form [9, 10]

$$\sigma_{\text{cont}} = \frac{1 - 2\nu_m}{3\pi} \left[6P \left(\frac{E}{R} \right)^2 \right]^{1/3}. \quad (9)$$

The Young's modulus E is derived as

$$\frac{1}{E} = \frac{1 - \nu_s^2}{E_s} + \frac{1 - \nu_m^2}{E_m}, \quad (10)$$

where the Young's moduli E_s and E_m along with the Poisson's ratios ν_s and ν_m are related to the spheres and an investigated ceramic material, respectively.

4. Experimental materials and applied mechanical tests

4.1. Experimental materials

Mechanical tests presented in Section 4.2 were applied to the following monolithic and composite ceramic materials:

1. Si_3N_4 with additives of 3 % Al_2O_3 and 3 % Y_2O_3 , sintered in atmosphere of N_2 . Si_3N_4 was produced by CeramTec (Plochingen, Germany), and provided in a form of plates with the dimensions $47 \times 11 \times 102$ (mm³).

2. SiC prepared as a mixture of the commercially available β -SiC powder (HSC-0.59, Superior Graphite) with additives of 2.8 % Al_2O_3 , 5.7 % Y_2O_3 , and 5 % Si_3N_4 , hot pressed at 1870 °C/1 hour in atmosphere of N_2 , and subsequently annealed at 1650 °C/5 hours. SiC was produced by the Institute of Inorganic Chemistry, Slovak Academy of Sciences in Bratislava, and provided in a form of plates with the dimensions $60 \times 60 \times 6$ (mm³).

3. The MoSi_2 + 10 % SiC composite, produced by Cesiwid, Erlangen, Germany, and provided in a form of prisms with the dimensions $3 \times 4 \times 45$ (mm³).

4.2. Preparation of samples and material analysis

Specimens used for the mechanical tests were cut by diamond tools, ground and consequently polished with 1 μm finish. The specimen edges were chamfered to the radius 0.15 mm to minimize a stress concentration influence. A number of the specimens used for the following mechanical tests are 10–30.

A power-driven diamond cut-off wheel performed the sectioning for a microstructural analysis of the investigated materials, and the hot-mounting process

was applied to all investigated materials. Two-step planar grinding for rapid removal of the materials was realized by semi-automatic equipment. Considering the first step, the planar grinding was performed at a load of 120–150 N and rotational speed of 120–300 rpm. Considering the second step to represent fine grinding, a load was decreasing within a range of 60–90 N in order to reduce pullouts and improve quality of a surface of samples. The two-step grinding was followed by mechanical polishing to use diamond suspensions with grain size of 9, 6, 3, 1 μm .

Chemical or thermal methods of subsequent etching of the polished surfaces were required to be applied at small increments until the most suitable etching conditions were determined [11]. These methods were applied in order to obtain an evenly attacked surface suitable for the microstructural analysis. The microstructural analysis was performed by optical and scanning electron microscopy, and grain size to include an aspect ratio was determined by the software Image J.

The four-point bending test as well as the contact test using rollers and spheres broke specimens for a fractographical analysis of the investigated materials. The broken specimens were investigated for the determination of a failure source to be either extraneous natural flaws or indentations. Pores and porous regions represented the flaws considered to be a fracture origin. Agglomerates, inclusions, compositional inhomogeneities and large grains, all representing common flaws to originate during the processing, were observed at the four-point bending test. In contrast to the contact test using rollers (see Section 3.2), fracture paths to originate during the contact test using spheres could not be identified due to the destruction of specimens to pieces. A study of fracture surfaces was performed by optical and scanning electron microscopy.

The specimens to be loaded without their failure (see Section 4.3) were cut through a centre of a contact surface, ground and polished due to the optical and electron microscopy. In this case, the optical and electron microscopy was used for the determination of the length c and the angle α of a crack. The angle α was measured between the crack and the contact surface (see Fig. 3). Consequently, the determination of c and α was performed by the software Image J [12].

4.3. Mechanical tests

The ceramic materials presented in Section 4.1 (see Items 1–3) were investigated by the following mechanical tests:

- the four-point bending test (see Section 3.1),
- the single-cycle contact test using rollers (see Section 3.2),
- the single-cycle contact test using spheres (see Section 3.3).

Table 1. The Young's modulus E_q and the Poisson's ratio ν_q for spheres ($q = s$) and experimental material ($q = m$)

Spheres	E_s (GPa)	ν_s
Standard hardened steel	200	0.29
WC	691.1	0.24
Experimental material	E_m (GPa)	ν_m
Si ₃ N ₄	310	0.24
SiC	400	0.2
MoSi ₂ + 10 % SiC	288.9	0.167

The four-point bending test was performed by the testing machine Lloyd LR 5KPLUS at the outer and inner spans, $S_1 = 40$ mm and $S_2 = 20$ mm (see Fig. 1), respectively, at room temperature and a loading rate of 0.5 mm min⁻¹, applied to specimens with the dimensions $W \times t \times L = 3 \times 4 \times 45$ (mm³).

The single-cycle contact test using rollers of standard hardened steel with the diameter $D = 3$ mm was performed by the testing machine Lloyd LR 5KPLUS at room temperature, and applied to specimens with the dimensions $W \times t \times L = 3 \times 4 \times (10-15)$ (mm³) (see Fig. 2). The test was performed in such a way that the load P was increased with a loading rate of 0.5 mm min⁻¹ up to the critical value P_c to cause failure of specimens.

The single-cycle contact test using spheres of the standard hardened steel with the radius $R = 2, 2.5, 3.5$ mm was also performed by the testing machine Lloyd LR 5KPLUS at room temperature and a loading rate of 0.5 mm min⁻¹, applied to specimens with the dimensions $W \times t \times L = 3 \times 4 \times 25$ (mm³) (see Fig. 3). A part of specimens was tested by the load P increasing to the critical value P_c to cause failure of specimens. A rest of specimens was tested by an increasing load to be stopped at $P = 4.9$ kN reached before the critical value P_c , i.e. before failure of specimens, with an aim to investigate a character and parameters of cracks to originate during the loading. The strength σ_{cont} (see Eqs. (9), (10)) for the determination of the characteristic strength $\sigma_{0,\text{cont}}$ derived by the Weibull analysis (see Section 2) considers the material parameters presented in Table 1.

5. Results and discussion

5.1. Microstructural analysis

Microstructure of the Si₃N₄ monolith (see Fig. 4a) consists of moderately elongated β -Si₃N₄ grains with the aspect ratio 3–5. Additionally, the inter-granular

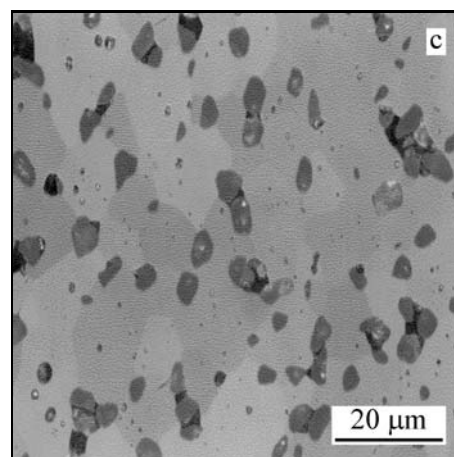
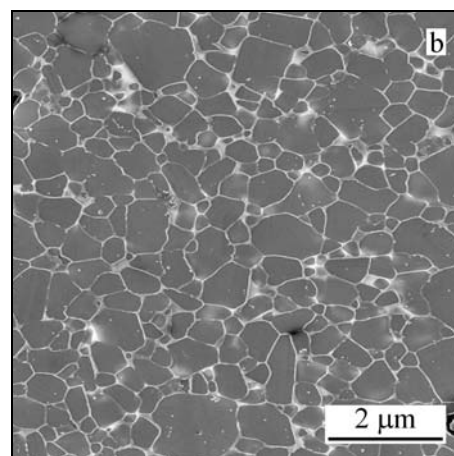
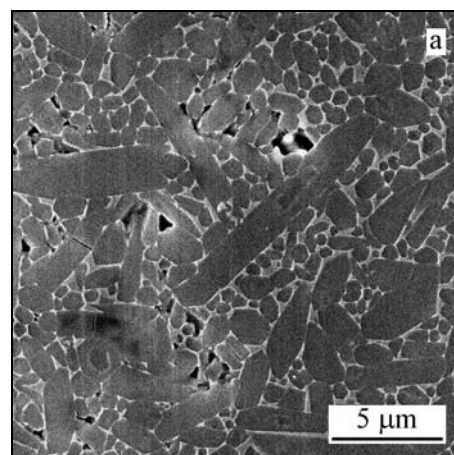


Fig. 4. SEM micrographs of microstructure of Si₃N₄ plasma etched (a), SiC plasma etched (b), and MoSi₂ + 10 % SiC thermally etched (c).

glassy phase with the volume fraction 12 %, and small amount (i.e. 0.03–0.16 wt.%) of α -Fe grains to remain from original powder used within the processing are also present.

Microstructure of the SiC monolith (see Fig. 4b) consists of fine sub-micron equiaxed SiC grains with

Table 2. The characteristic strength $\sigma_{0,\text{cont}}$ and $\sigma_{0,\text{bend}}$ along with the Weibull moduli m_{cont} and m_{bend} determined by the Weibull distributions of σ_{cont} (MPa) (see Eq. (7)) and σ_{bend} (MPa) (see Eq. (5)) in Fig. 5a and Fig. 5b related to the single-cycle contact test using rollers and the four-point bending test, respectively

Material	$\sigma_{0,\text{cont}}$ (MPa)	$\sigma_{0,\text{bend}}$ (MPa)	$\sigma_{0,\text{cont}}/\sigma_{0,\text{bend}}$	Eq. (6)
Si ₃ N ₄	766.3	727.8	1.05	1
SiC	617.1	437.1	1.41	1
	m_{cont}	m_{bend}	$m_{\text{bend}}/m_{\text{cont}}$	Eq. (8)
Si ₃ N ₄	7.1	13.9	1.96	2
SiC	8.95	10.6	1.18	2

a low aspect ratio and average size of 450 nm. No effect of heat treatment at 1650 °C was found on microstructure of SiC. All components remaining from original powder are present in a form of very thin intergranular phases. Additionally, triple points with a size up to 0.5 μm are also observed.

The MoSi₂ + 10 % SiC composite (see Fig. 4c) with the porosity of 3.2 vol.% contains SiC grains with average size of 5 μm and clusters of the SiC grains. The MoSi₂ grains representing a matrix of MoSi₂ + 10 % SiC exhibit size of 10–15 μm .

5.2. Mechanical tests

5.2.1. Single-cycle contact test using rollers

The characteristic strength $\sigma_{0,\text{cont}}$, $\sigma_{0,\text{bend}}$, the Weibull moduli m_{cont} , m_{bend} , and the ratios $m_{\text{bend}}/m_{\text{cont}}$, $\sigma_{0,\text{cont}}/\sigma_{0,\text{bend}}$ are presented in Table 2. $\sigma_{0,\text{cont}}$, m_{cont} and $\sigma_{0,\text{bend}}$, m_{bend} related to the single-cycle contact test using rollers and to the four-point bending test are determined by the Weibull distributions of σ_{cont} (see Eq. (7)) and σ_{bend} (see Eq. (5)) in Fig. 5a and Fig. 5b, respectively.

Si₃N₄ exhibits the ratios $\sigma_{0,\text{cont}}/\sigma_{0,\text{bend}} \approx 1$, $m_{\text{bend}}/m_{\text{cont}} \approx 2$ which fulfil the Fett's theory (see Eqs. (6), (8)), in contrast to $\sigma_{0,\text{cont}}/\sigma_{0,\text{bend}} \approx 1$, $m_{\text{bend}}/m_{\text{cont}} \approx 2$ for SiC. A low value of $\sigma_{0,\text{bend}}$ compared with $\sigma_{0,\text{cont}}$ for SiC is assumed to be caused by the presence of relatively large flaws in a form of small pores or clusters of pores with a diameter of 5–10 μm (see Fig. 6a–c). Additionally, the processing flaws located in volume of SiC are a reason of low values of m_{bend} , $m_{\text{bend}}/m_{\text{cont}}$, and $\sigma_{0,\text{cont}}/\sigma_{0,\text{bend}}$. In contrast to SiC, processing flaws in Si₃N₄ loaded (see Fig. 6d) are located on the specimen surface and the specimen edges.

As shown in Fig. 7, a stress state induced by the single-cycle contact test using roller results in the initiation and subsequently the propagation of different types of cracks, i.e. lateral (L), median (M) and contact end (C) cracks. However, all of the cracks are not observed to arise in all of specimens of the same material. At the very beginning, the lateral crack arises

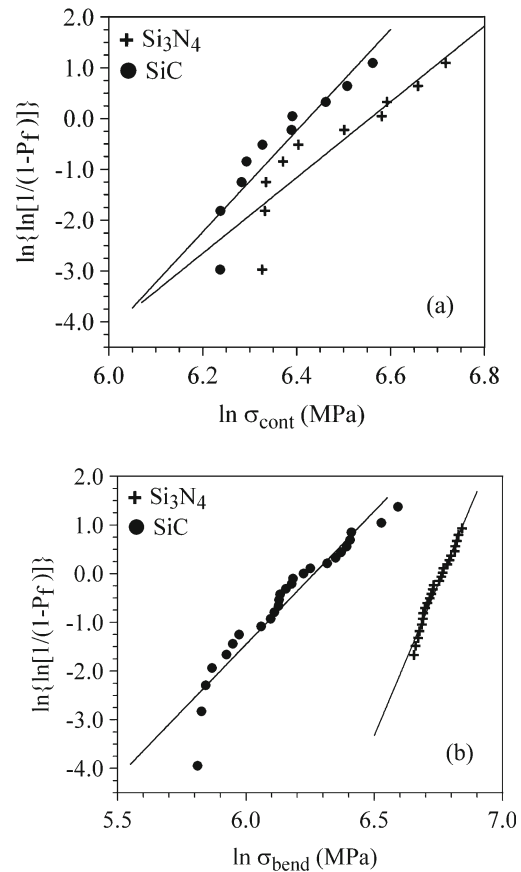


Fig. 5. The Weibull distribution of the strength σ_{cont} (MPa) (see Eq. (7)) (a) and σ_{bend} (MPa) (see Eq. (5)) (b) related to the contact test using rollers and to the four-point bending test for the investigated materials, respectively.

below one or both of contact surfaces in depth equal to $(2 - 4) \times a$, and exhibits a slight concave shape with edges towards the contact surface.

Consequently, the median crack perpendicular to the contact surface is propagated from the lateral crack to the contact mark, reaching the contact surface at the contact end crack. The contact end crack initiated on the contact surface tends to propagate to the specimen sides. Subsequently, the contact

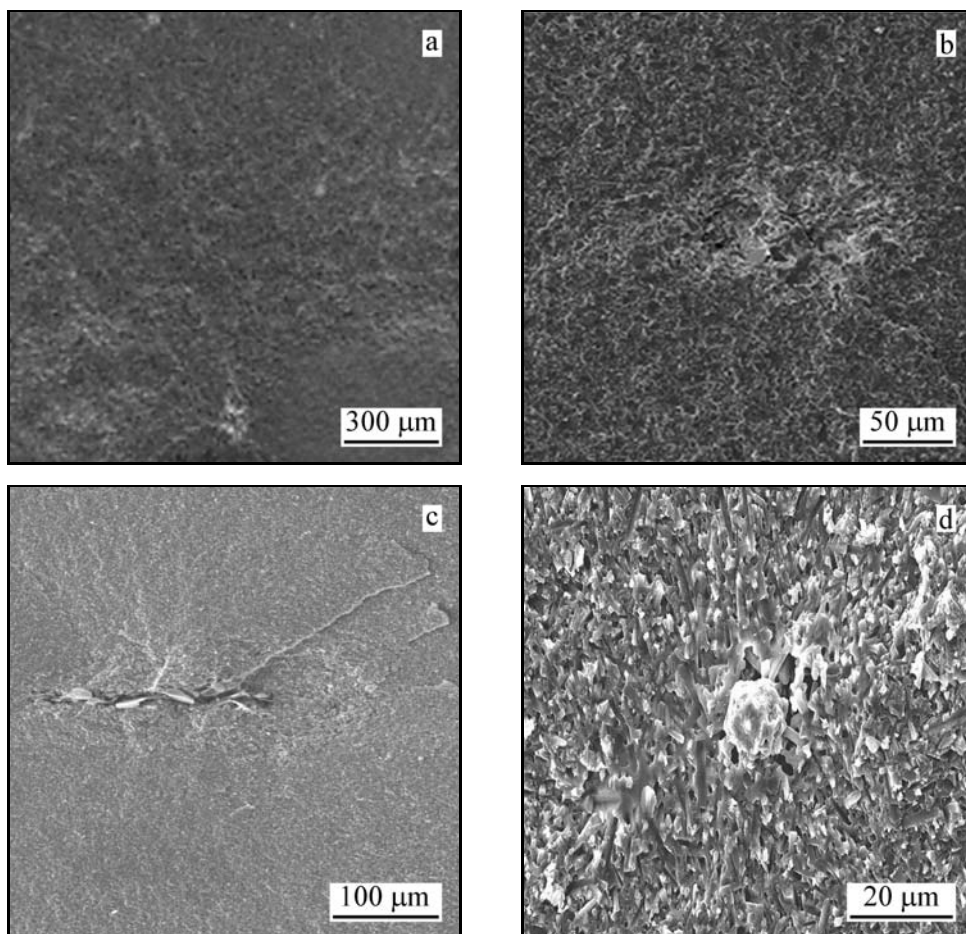


Fig. 6. Fracture surfaces of the investigated materials loaded by the four-point bending test. Fracture origin in SiC (a) and details of the fracture origins in SiC (b, c) and Si₃N₄ (d).

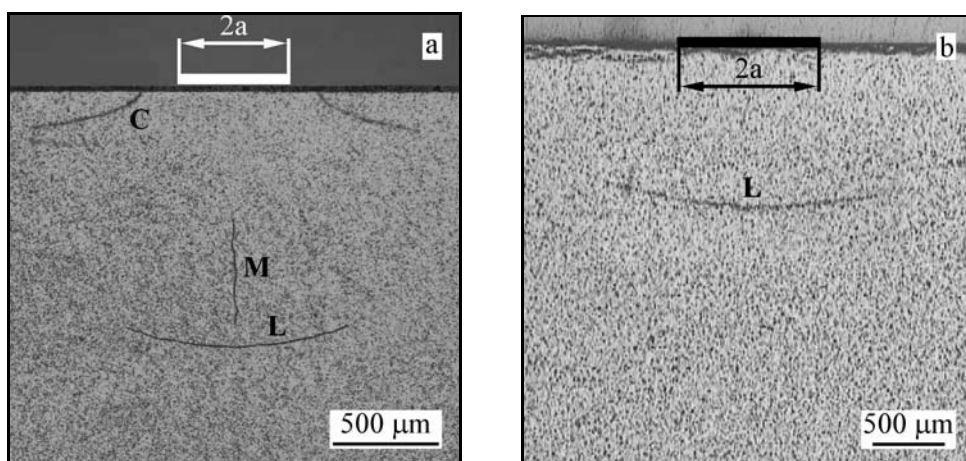


Fig. 7. Cross-sections of a surface between two rollers: the lateral (L), median (M) and contact end (C) cracks in Si₃N₄ (a), and the lateral (L) crack in SiC (b), where a is a radius of a contact surface.

end crack exhibits a direction parallel to the contact surface with the tendency to be curved to the contact edge (see Fig. 7a). Critical size of the contact end crack is assumed to be a primary reason of the degradation of strength and material failure

[13]. The same types of cracks, i.e. the lateral, median and contact end cracks, arising probably as a consequence of a non-homogeneous stress state, are formed within the contact fatigue test applied to steel [13].

Table 3. The characteristic strength $\sigma_{0,\text{cont}}$ and $\sigma_{0,\text{bend}}$ along with the Weibull moduli m_{cont} and m_{bend} determined by the Weibull distributions of σ_{cont} (MPa) (see Eqs. (9), (10)) and σ_{bend} (MPa) (see Eq. (5)) in Figs. 8a,b and 8b, related to the single-cycle contact test using spheres with the radius $R = 2.5$ mm and to the four-point bending test, respectively, where values of $\sigma_{0,\text{bend}}$, σ_{bend} for Si_3N_4 , SiC are taken from Table 2

Material	$\sigma_{0,\text{cont}}$ (MPa)	$\sigma_{0,\text{bend}}$ (MPa)	m_{cont}	m_{bend}
Si_3N_4	3344.2	727.8	22.6	13.9
SiC	3327.6	437.1	20.5	106
$\text{MoSi}_2 + 10\% \text{ SiC}$	2048.8	225.9	92.5	5.4

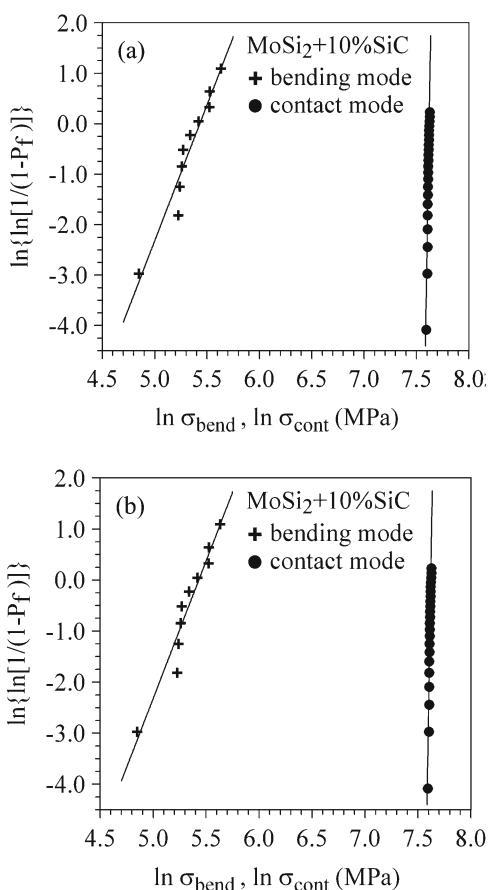


Fig. 8. The Weibull distribution of the strength σ_{cont} (MPa) (see Eqs. (9), (10)) (a, b) and σ_{bend} (MPa) (see Eq. (5)) (b) related to the contact test using spheres with the radius $R = 2.5$ mm and to the four-point bending test for the investigated materials, respectively.

5.2.2. Single-cycle contact test using spheres

The characteristic strengths $\sigma_{0,\text{cont}}$, $\sigma_{0,\text{bend}}$ along with the Weibull moduli m_{cont} , m_{bend} are presented in Table 3. $\sigma_{0,\text{cont}}$, m_{cont} and $\sigma_{0,\text{bend}}$, m_{bend} related to the single-cycle contact test using spheres with the radius $R = 2.5$ mm and to the four-point bending test are determined by the Weibull distributions of σ_{cont} (MPa) (see Eqs. (9), (10)) and σ_{bend} (MPa) (see Eq. (5)) in Figs. 8a,b and 5b, 8b, respectively.

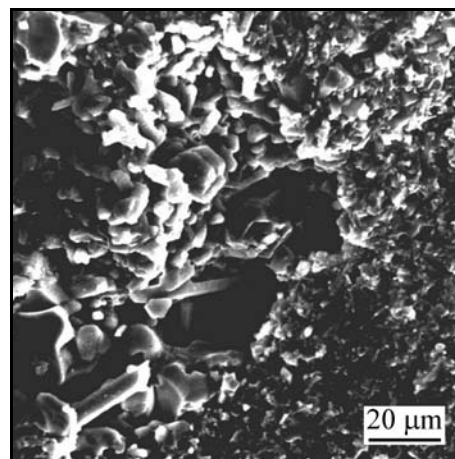


Fig. 9. Fracture origins in $\text{MoSi}_2 + 10\% \text{ SiC}$.

With regard to m_{cont} in Table 3 to be higher than m_{cont} in Table 2, the single-cycle contact test using spheres can be considered to be the most precise and accordingly the most considerable for the determination of strength of ceramic materials. Additionally, considering the significant difference $\sigma_{0,\text{cont}} - \sigma_{0,\text{bend}}$ in Table 3, the preciseness can be explained by stable growth of cone cracks [14–16], and not by an initial size distribution of flaws. In case of $\text{MoSi}_2 + 10\% \text{ SiC}$, the flaws in a form of pores are located in volume of this material (see Fig. 9).

Si_3N_4 and $\text{MoSi}_2 + 10\% \text{ SiC}$ are characterized by the highest and lowest fracture toughness, respectively, and SiC exhibits medium fracture toughness [7]. Consequently, $\text{MoSi}_2 + 10\% \text{ SiC}$ to be very brittle exhibits lowest values of $\sigma_{0,\text{bend}}$, m_{bend} (see Table 3). Additionally, the following analysis concerning thermal stresses in the $\text{MoSi}_2 + 10\% \text{ SiC}$ composite might be considered. With regard to $\alpha_{\text{MoSi}_2} > \alpha_{\text{SiC}}$, the MoSi_2 matrix of the MoSi_2 -SiC matrix-particle system is acted by compressive radial and tensile tangential thermal stresses, where α_{MoSi_2} and α_{SiC} are thermal expansion coefficients of the MoSi_2 matrix and the SiC particle [17], respectively. Accordingly, the compressive radial and tensile tangential stresses represent a contribution to tensile stresses induced on a tensile surface of a specimen loaded by

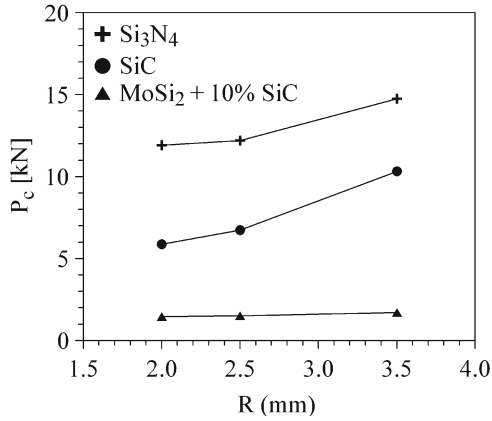


Fig. 10. The critical load P_c versus the radius R of spheres of the contact test for $R = 2, 2.5, 3.5$ mm.

the four-point bending test. Additionally, a surface of flaws located in the MoSi_2 matrix of the MoSi_2 -SiC matrix-particle system is influenced by the compressive thermal stresses oriented to the flaw centre. In general, the crack propagation due to the presence of the flaws is caused by tensile stresses. The tensile stresses represent a part of the non-homogeneous compressive-tensile stress state induced by the single-cycle contact test using spheres. However, the flaws are pressed by the surface compressive radial thermal stresses. The surface compressive radial thermal stresses are thus assumed to represent resistance against the tensile stresses, and consequently against the crack propagation from the flaw surface. Finally, the resistance might be a reason of a significantly higher value of $\sigma_{0,\text{cont}}$ compared with a value of $\sigma_{0,\text{bend}}$.

As shown in Fig. 10, the critical load by P_c as a reason of failure of a specimen is an increasing function of the radius R of spheres. A smaller radius to result in a smaller contact surface is a reason of a higher “concentration” of stresses, i.e. higher gradients of stresses induced in a specimen by the load P . The higher gradients are assumed to result in a lower value of the critical load P_c , and vice versa.

Finally, the crack length $c = c(R)$ and the angle α (see Fig. 11) represent decreasing and increasing functions of the radius R due to the higher “concentration” and the smaller gradients at smaller and higher R , respectively. The smaller “concentration” and the smaller gradients at higher R result in a more homogeneous stress state close to the normal to a contact surface, where the normal is related to a centre of the contact surface.

The decreasing and increasing functions $c = c(R)$ and $\alpha = \alpha(R)$ of the radius R arise from experimental results in Fig. 12 to present optical micrographs of cross-sections of contact sites in Si_3N_4 (see Fig. 12a,b) and SiC (see Fig. 12c,d).

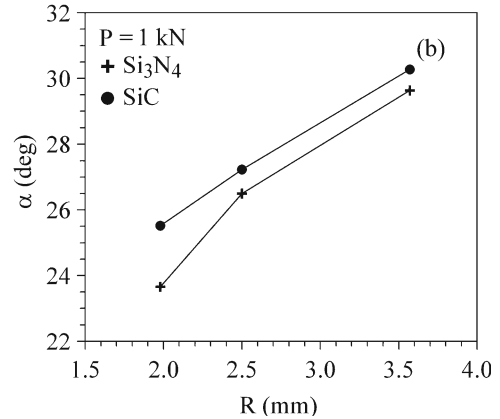
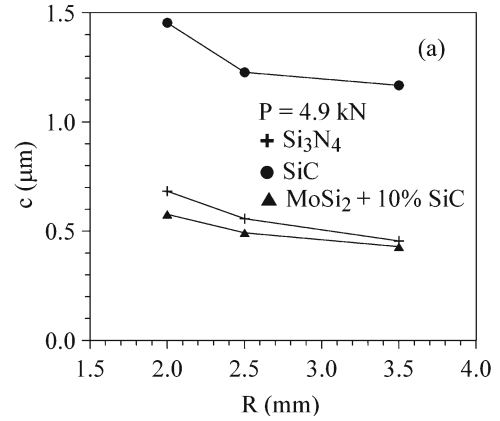


Fig. 11. The crack length c (a) and the angle α (b) versus the radius R of spheres of the contact test for $R = 2, 2.5, 3.5$ mm, $P = 4.9$ kN (a), $P = 1$ kN (b).

The cone cracks in Si_3N_4 and SiC (see Figs. 12a–d) propagated from the contact surface exhibited a perpendicular course below the contact surface (5–10 μm). The perpendicular course is followed by a linear course with length of 200–500 μm . Additionally, a radius of the cone cracks in planes parallel to the contact surface increases with the increase of R (see Figs. 12a–d). On the contrary, quasi-parallel multiple cone cracks in SiC with a lower radius than that in Si_3N_4 are assumed to propagate independently on each other. The crack propagation arises from and below the contact surface regarding to a lower and higher sphere radius, i.e. for $R = 2$ mm and $R = 2.5$ mm, as shown in Fig. 12c and Fig. 12d, respectively. Additionally, the cracks to propagate below the contact surface for $R = 2.5$ mm exhibit a concave course regarding a plane in the specimen centre, parallel to the contact surface. Strictly speaking, the cone crack course is convex regarding the contact surface (see Fig. 12d).

Si_3N_4 is tougher than SiC, and accordingly the contact surface between spheres and SiC exhibits higher deformation of the spheres. Finally, the higher deformation of the spheres is assumed to be a reason of the formation of the quasi-parallel multiple cone cracks.

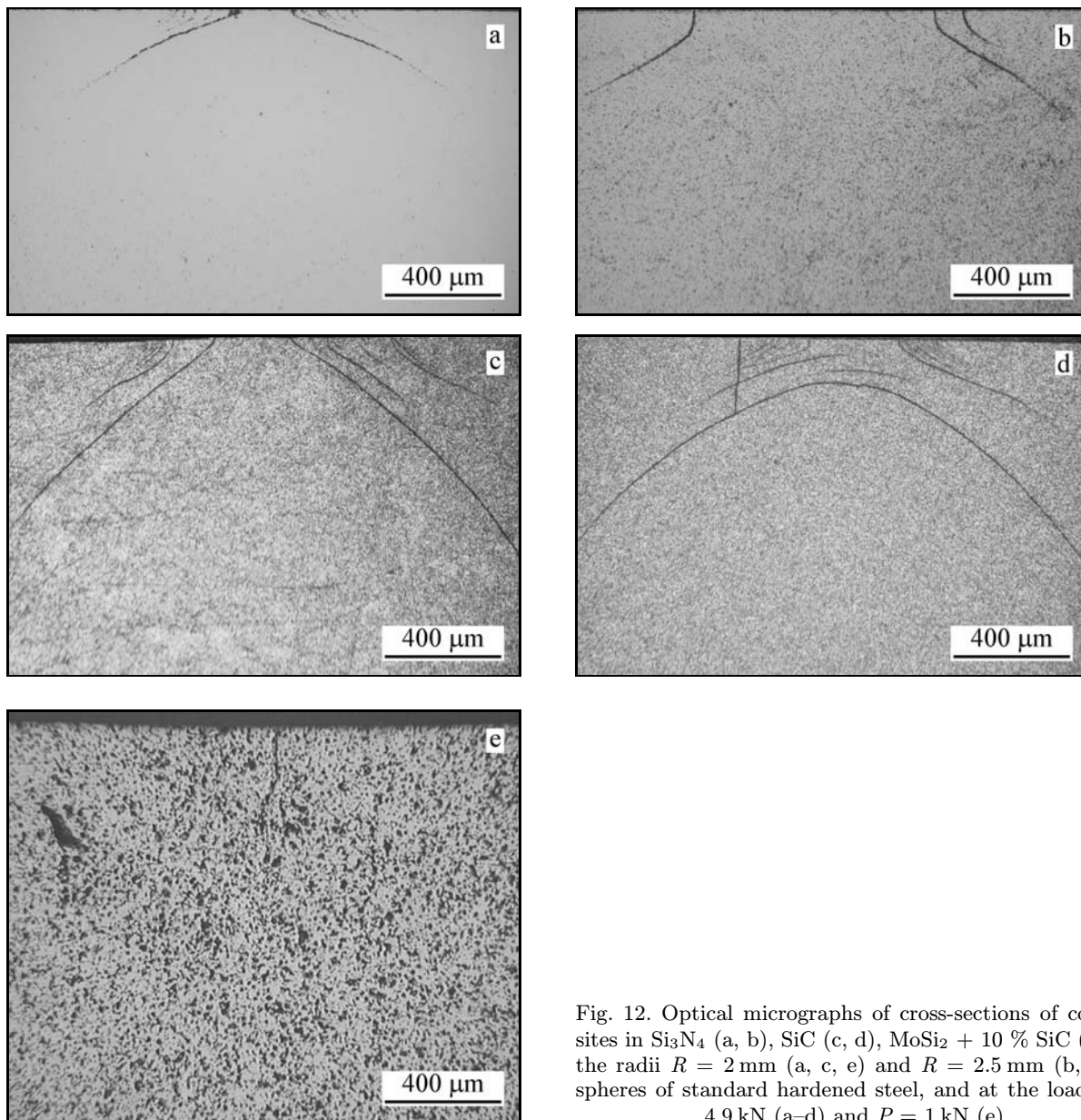


Fig. 12. Optical micrographs of cross-sections of contact sites in Si_3N_4 (a, b), SiC (c, d), $\text{MoSi}_2 + 10\% \text{SiC}$ (e) for the radii $R = 2 \text{ mm}$ (a, c, e) and $R = 2.5 \text{ mm}$ (b, d) of spheres of standard hardened steel, and at the load $P = 4.9 \text{ kN}$ (a–d) and $P = 1 \text{ kN}$ (e).

Figure 12e shows optical micrographs of cross-sections of contact sites in $\text{MoSi}_2 + 10\% \text{SiC}$, where no cone cracks are observed. The median crack perpendicular to the contact surface in $\text{MoSi}_2 + 10\% \text{SiC}$ is assumed to correspond to shear-fault/wing cracks propagated in a quasi-plastic material [18, 19]. In general, brittle ceramic materials are characterized by a wider interval of the characteristic strength σ_0 and consequently a lower value of the Weibull modulus m . This is in contrast to plastic and quasi-plastic materials characterized by a narrow interval of σ_0 to result in a high value of m . On the one hand, as analysed above, $\text{MoSi}_2 + 10\% \text{SiC}$ exhibits low values of $\sigma_{0,\text{bend}}$, m_{bend} . These low values might be a consequence of the presence of flaws located in volume of $\text{MoSi}_2 + 10\% \text{SiC}$, as well as

a consequence of the thermal stresses acting in this material. On the other hand, with regard to a compressive stress state as a part of the non-homogeneous compressive-tensile stress state induced by the contact test, the $\text{MoSi}_2 + 10\% \text{SiC}$ composite material might be considered to represent a quasi-plastic material. Finally, the quasi-plastic character results in a high value of m_{cont} compared with those of Si_3N_4 and SiC.

6. Conclusions

Results of the single-cycle contact test using rollers and of the four-point bending test are as follows:

1. Si_3N_4 exhibits the ratios $\sigma_{0,\text{cont}}/\sigma_{0,\text{bend}} \approx 1$,

$m_{\text{bend}}/m_{\text{cont}} \approx 2$ to fulfil the Fett's theory represented by Eqs. (6), (8). The failure of Si_3N_4 is caused by the presence of processing flaws located in a form of small defects on surfaces and at edges of a specimen.

2. SiC exhibits the ratios $\sigma_{0,\text{cont}}/\sigma_{0,\text{bend}} \approx 1$, $m_{\text{bend}}/m_{\text{cont}} \approx 2$ not to fulfil the Fett's theory (see Eqs. (6), (8)). The failure of SiC is a consequence of the presence of relatively large processing flaws in a form of small pores or clusters of pores located in volume of a specimen.

3. In contrast to the specimen failure induced by the four-point bending test, the single-cycle contact test using rollers results in the specimen failure to be a consequence of different types of cracks, i.e. the lateral, median and contact end cracks.

Results of the single-cycle contact test using spheres and of the four-point bending test are as follows:

1. The single-cycle contact test using spheres exhibits higher values of m_{cont} compared with those of both the single-cycle contact test using rollers and the four-point bending test. This test is assumed to be the most precise and accordingly the most considerable for the determination of strength of ceramic materials.

2. Significantly low values of $\sigma_{0,\text{bend}}$ compared with those of $\sigma_{0,\text{cont}}$ are a consequence of a negative influence of flaws within the specimen bending. As mentioned in Section 5.2.1, the flaws are located in volume of SiC, and on surfaces and at the edge of a specimen of Si_3N_4 . In case of $\text{MoSi}_2 + 10\% \text{ SiC}$, the flaws located in volume of this material are assumed to be a reason of a low value of m_{bend} .

3. On the one hand, a low value of $\sigma_{0,\text{bend}}$ for $\text{MoSi}_2 + 10\% \text{ SiC}$ might result from thermal stresses originating in this material due to $\alpha_{\text{MoSi}_2} > \alpha_{\text{SiC}}$. On the other hand, the thermal stresses might be a reason of a significantly higher value of $\sigma_{0,\text{cont}}$ compared with a value of $\sigma_{0,\text{bend}}$.

4. The critical load P_c as a reason of failure of a specimen is an increasing function of the radius R of spheres.

5. The length $c = c(R)$ of a cone crack and the angle $\alpha = \alpha(R)$ between the cone crack and a contact surface represent decreasing and increasing functions of the radius of spheres, R , respectively.

6. Si_3N_4 and SiC exhibit cone cracks except the $\text{MoSi}_2 + 10\% \text{ SiC}$ composite which exhibits a median crack perpendicular to a contact surface.

Acknowledgements

This work was supported by the Slovak Research and Development Agency under the contracts No. APVV-COST-0042-06, No. APVV-0034-07, No. APVV-0171-06, No. APVV LPP-0203-07; No. APVV LPP 0174-07; by HANCOC-MNT.ERA-NET 01/09-12/11; by NANO-SMART Centre of Excellence (1/1/2007-31/12/2010) Slovak Academy of Sciences; by the Slovak Grant Agency VEGA No. 2/7194/27, No. 2/7171/27; No. 2/0088/08; and by COST Action 539.

References

- [1] PÁLKA, V.—POŠTRKOVÁ, E.—KRSEK, A.—LIPA, Z.: *Kovove Mater.*, 35, 1997, p. 400.
- [2] HVIZDOŠ, P.—RUDNAYOVÁ, E.—DUSZA, J.—BARINOV, S. M.—KRYLOV, A. V.: *Kovove Mater.*, 34, 1996, p. 133.
- [3] REINISCH, M.—VLACH, B.—TRUNEC, M.: *Kovove Mater.*, 34, 1996, p. 44.
- [4] HVIZDOŠ, P.—LOFAJ, F.—DUSZA, J.: *Kovove Mater.*, 33, 1995, p. 473.
- [5] RUDNAYOVÁ, E.—HVIZDOŠ, P.—DUSZA, J.—ŠAJGALÍK, P.—LENCÉŠ, Z.: *Kovove Mater.*, 33, 1995, p. 281.
- [6] HEGEDÚSOVÁ, L.—KOVALČÍKOVÁ, A.—DUSZA, J.: *Kovove Mater.*, 46, 2008, p. 377.
- [7] SKOČOVSKÝ, P.—BOKŮVKA, O.—PALČEK, P.: *Materials Science. Žilina, EDIS Technical University 1996.*
- [8] FETT, T.—ERNST, E.—MUNZ, D.—BADENHEIM, D.—OBERACKER, R.: *J. Eur. Ceram. Soc.*, 23, 2003, p. 2031.
- [9] FETT, T.—MUNZ, D.: *Eng. Fract. Mech.*, 69, 2002, p. 1353.
- [10] FETT, T.—MUNZ, D.—THUN, G.: *Strength and Toughness Test Devices with Opposite Roller Loading. Report FZKA 6378. Karlsruhe, Forschungszentrum 2000.*
- [11] AUDY, J.—AUDY, K.: *Pract. Metallography*, 45, 2008, p. 101.
- [12] <http://www.rsbweb.nih.gov/ij>
- [13] ALFREDSSON, B.—OLSSON, M.: *Fatigue Fract. Eng. Mater. Struct.*, 22, 1999, p. 225.
- [14] FETT, T.—ERNST, E.—MUNZ, D.: *J. Mater. Sci. Lett.*, 21, 2002, p. 1955.
- [15] EGGENBERGER, G.—IVANČO, V.—KOSTOLNÝ, K.: *Comput. Mater. Sci.*, 37, 2006, p. 599.
- [16] AUDY, J.: *J. Mater. Process. Technol.*, 204, 2008, p. 130.
- [17] CENIGA, L.: *Analytical Models of Thermal Stresses in Composite Materials I. New York, Nova Science Publishers 2008.*
- [18] LAWN, B. R.—LEE, S. K.—PETERSON, I. M.—WUTTIPHAN, S. J.: *J. Amer. Ceram. Soc.*, 81, 1998, p. 1509.
- [19] LEE, S. K.—LAWN, B. R.: *J. Amer. Ceram. Soc.*, 81, 1998, p. 997.